Talanta 248 (2022) 123579

Contents lists available at ScienceDirect

Talanta

journal homepage: www.elsevier.com/locate/talanta

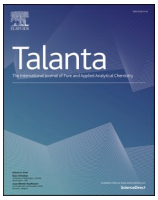

Optimization of flow path parameters for enhanced sensitivity lateral flow devices

Alice H. Iles *, Peijun J.W. He, Ioannis N. Katis, Peter Horak, Robert W. Eason, Collin L. Sones

Optoelectronics Research Centre, University of Southampton, SO17 1BJ, UK

ARTICLE INFO

Keywords:
Flow
High sensitivity
Lateral flow
High sensitivity lateral Flow device (HS-LFD)
Geometric
Flow dynamics

ABSTRACT

Lateral flow devices (LFDs) or lateral flow tests (LFTs) are one of the most widely used biosensor platforms for point-of-care (POC) diagnostics. The basic LFD design has remained largely unchanged since its first appearance, and this has limited LFD use in clinical applications due to a general lack of analytical sensitivity. We report here a comprehensive study of the use of laser-patterned geometric control barriers that influence the flow dynamics within an LFD, with the specific aim of enhancing LFD sensitivity and lowering the limit of detection (LOD). This control of sample flow produces an increase in the time available for optimizing the binding kinetics of the implemented assay. The geometric modification to the flow path is in the form of a constriction that is produced by depositing a photo-sensitive polymer onto the nitrocellulose membrane which when polymerized, creates impermeable barrier walls through the depth of the membrane. Both the position of the constriction within the flow path and the number of constrictions allow for an increase in the sensitivity because of a slower overall flow rate within the test and a larger volume of sample per unit width of the test line. For these high sensitivity LFDs (HS-LFD), through optimization of the constriction position and addition of a second constriction we attained a 62% increase in test line color intensity for the detection of procalcitonin (PCT) and were also able to lower the LOD from 10 ng/mL to 1 ng/mL. In addition, of relevance for future commercial exploitation, this also significantly decreases the antibody consumption per device leading to reduced costs for test production. We have further tested our HS-LFD with contrived human samples, validating its application for future clinical use.

1. Introduction

The rapid, specific, sensitive, and cost-effective detection of analytes from complex samples is essential for in vitro diagnostics [1], and it is estimated that improving diagnostic testing for infectious diseases in developing countries could prevent 1.2 million deaths annually [2]. This has recently been brought into stark relief by the current severe acute respiratory syndrome coronavirus 2 (SARS-CoV-2) pandemic. A rapid and simple screening strategy, employed in airports, customs, and the community, was instrumental in preventing further disease spread, thereby helping resume economic development. Lateral flow devices (LFDs) deployed as point-of-care (POC) tests, are rapid, stable and portable [3], and have been vital in enabling faster diagnosis, directing medical interventions, and mitigating the transmission of infectious diseases.

LFDs are constructed from different porous membranes, each with their own specific properties. The nitrocellulose membrane for example is used for the reaction zone as it facilitates the immobilization of the capture antibodies that form the test and control lines of the LFD. The conjugate pad enables the rehydration of pre-deposited detection antibodies as the liquid sample is introduced to the LFD and the wicking pad removes excess reagents and background interference from the test. The sample and other reagents are transported by capillary action within these porous materials and therefore no external pump or equipment is required to run the test. Although LFDs are capable of supporting multiple immunoassay formats, the most commonly employed is the sandwich immunoassay, as used within this report. The analyte in the sample initially binds to a detection antibody labelled with a colored (often gold) nanoparticle for visualization. This complex is transported along the flow path of the LFD to the capture antibody site which is specific to the analyte and is immobilized on the nitrocellulose membrane in the form of a test line. The accumulation of such capture-analyte-detection antibody complexes is then visible as a red colored test line that can be measured qualitatively by eye or quantitatively by using a reader. In addition to the test line, a control line is also used to confirm that the assay has worked and that all reagents have successfully travelled the

* Corresponding author.
E-mail address: a.iles@soton.ac.uk (A.H. Iles).

https://doi.org/10.1016/j.talanta.2022.123579
Received 10 March 2022; Received in revised form 17 May 2022; Accepted 19 May 2022
Available online 25 May 2022
0039-9140/© 2022 Published by Elsevier B.V.

full length of the LFD. Surplus reagents and buffers are transported toward the final wicking pad that collects unwanted/unused waste.

Standard LFDs produce a visual readout that can be identified with the naked eye to present a positive or negative answer. This is a simple detection strategy delivering rapid results, and pregnancy tests are an excellent and well-known example of this widely used process. However, such test results are qualitative, and in some cases, lack the necessary sensitivity for certain applications. For example, some critical biomarkers are present in extremely small concentrations in patient samples and these tests do not afford sufficient sensitivity and limit of detection (LOD), which have restricted their wider application. Of critical importance to achieving the optimal performance of an LFD is the balance between the reaction times needed or given for binding firstly between the analyte in the sample and the detection antibody and secondly the interaction and binding of this complex with the capture antibody pre-deposited at a test line [4]. For the latter, ensuring that sufficient time is given for this binding and that the maximum quantity of the sample-detection antibody complexes traverse the test line at a velocity that will ensure optimum binding with the capture antibodies presents other challenge that must be solved.

Although there has been significant research aimed at developing LFDs with enhanced performance, in terms of both increased sensitivity and lowered LOD, their optimization has largely been directed towards improvements and modifications of the biochemistry of the assay, use of membranes with different porosity, and the antibody labelling system, rather than deliberate and controlled optimization of local flow The conventional LFD design has not evolved for many years and therefore the efficiency of all such modifications remains limited by the basic unaltered architecture of the device. There is therefore a real need to identify fundamental architectural modifications that enhance both the LFD sensitivity and LOD. Work to date has addressed several strategies such as; geometric flow control within the nitrocellulose membrane by laser ablation to create a narrowing of the flow path and demonstrated a comprehensive exploration of flow control parameters including the width, length in addition to the input and output angle of the constriction [5]; a “stacking pad” configuration where an additional membrane is added between the conjugation pad and test pad that helps to accumulate the antibody and antigen on the stacking pad, extending the time available for the analyte/antibody binding to occur, thereby enhancing the test’s detection sensitivity [6]. Other proposed strategies include changing the architecture of an LFD to improve its sensitivity such as increasing the size of the sample and conjugate pad [7] or introducing wax pillars in the flow path to create an obstruction and thereby reduce the flow rate [8].

Building on our previous work [9], we now report the use of multiple constrictions within the flow path of the LFD, via precise laser-patterning of the nitrocellulose membrane to produce a high-sensitivity LFD and demonstrate its implementation for the detection of procalcitonin (PCT) an inflammatory marker that can be used for differentiating between bacterial and viral infections, making it a useful triage marker to guide the initiation and duration of antibiotic treatment. PCT has been approved by the US FDA for antimicrobial stewardship in the context of suspected sepsis as timely diagnosis and treatment is crucial for patient survival [10–13]. Procalcitonin can be measured in healthy patient serum with a range from <0.1 ng/mL to 0.5 ng/mL [14]; increasing above 0.5 ng/mL during systemic infection, levels of PCT above 0.5 ng/mL indicate that bacterial infection is very likely [11,15]. In addition, the levels of PCT have been shown to have predictive power of disease prognosis and likelihood of hospitalization of community-acquired pneumonia as well as death [16,17]. Patient PCT levels on their admission to hospital have a strong association with their APACH II score which is an ICU mortality prediction score [18].

2. Methods and materials

2.1. Materials

The LFDs were fabricated with backed nitrocellulose membrane purchased from Sartorius (UniSart CN95) and backing card purchased from Kenosha B.V, (Netherlands). The membrane thickness is 240–270 μm and has an average pore size of 0.45 μm and a capillary speed of 95 s/4 cm. The wicking pads were cellulose-based filter papers from GE Healthcare (CF4). The antibody used to produce the control line was an anti-mouse goat IgG from R&D Systems (AF007). The capture and biotinylated detection antibody for the PCT assay and the analyte were from the Human Procalcitonin DuoSet ELISA kit from R&D systems (DY8350). The streptavidin-conjugated gold nanoparticles (AuNPs), 40 nm, 10 OD, were obtained from Abcam (ab186864). BSA and PBS used in the solutions were obtained from Sigma Aldrich (A2058, P3813). The antibody used at the control line was donkey anti-sheep IgG antibody from R&D systems (BAF016). The samples were prepared using sterile filtered human serum obtained from Sigma Aldrich (H4522).

2.2. Laser direct-write patterning

To create the high-sensitivity LFDs, their flow path was constricted to a defined shape (schematically described in Fig. 1A) using a laser direct-write (LDW) approach that we have reported previously [19–21]. The constricted flow path is shaped such that its inlet gradually reduces in width over ~ 1 mm followed by 8 mm of constant 1 mm width leading to a 1 mm angled outlet where the flow path returns to the standard 4.5 mm width. We have already shown the versatility and usefulness of this LDW technique in the patterning of diagnostic devices in porous materials such as cellulose filter [22,23] and nitrocellulose membranes [21]. When implemented in multiplexed device formats we have shown that it can be used to create impermeable barriers that do not allow liquid to migrate between the multiple channels, therefore eliminating cross-reactivity [20].

There are several other methods that have been reported for the patterning of membranes including photolithography [24], wax printing [8,25–27], inkjet printing [28], laser cutting or ablation [5,29,30], flexographic printing [31] and plasma treatment [32,33]. In comparison, the LDW method exhibits key advantages: it does not need expensive and fixed patterning masks, custom equipment, specialist chemicals or inks which can also be hazardous and messy, it does not create debris, it does not require a solid or backed membrane as it uses lower power and performs faster, and it overcomes the limitation of lateral spreading of the hydrophobic material used to form the fluidic channel walls with barriers extending through the thickness of the membrane with dimensions below 100 μm. Most significantly it is suitable for scale-up to mass-production on a roll-to-roll basis for easy implementation into a LFD production line.

The schematic in Fig. 1A describes in more detail this LDW patterning protocol. A liquid photopolymer is first locally deposited onto the porous substrate via a dispensing nozzle at locations pre-defined by the device design, and for the case of a constricted LFD, this deposition involves creating polymer barriers within only the nitrocellulose membrane. A laser beam subsequently follows the same trajectory of the deposition head and illuminates the deposited polymer line pattern(s) thereby inducing photo-polymerization of the polymer, transforming it into a fully solidified polymeric wall that extends throughout the full depth of the membrane. The polymerized structures (with ~1 mm width) serve as impregnable demarcating barriers that define the boundaries of the constrictions within the LFDs to confine the liquid within their specified channel within the device. The speed used for deposition of the polymer lines on the porous substrate is a function of the thickness and porosity of the material, and for the nitrocellulose used was 50 mm/s and the laser speed used to illuminate (and thereby polymerize) the polymer was also 50 mm/s. A time delay of 15 s was

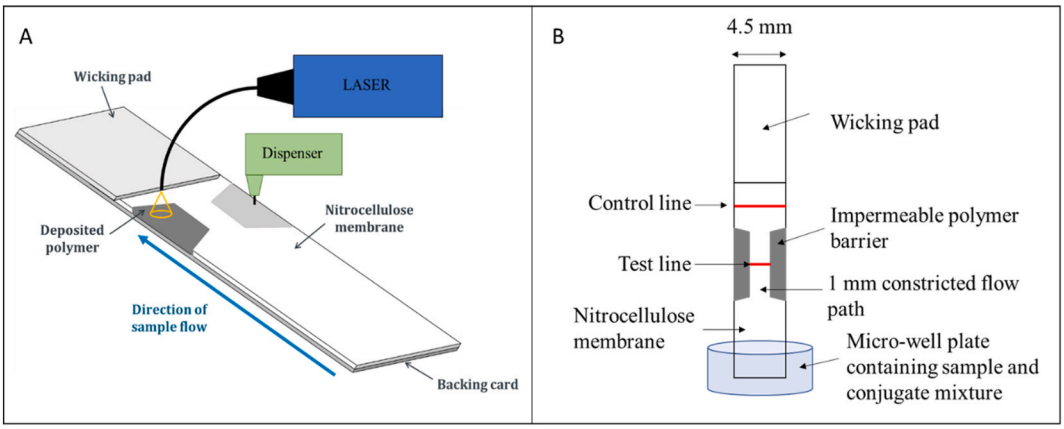

Fig. 1. A- Schematic of the laser-direct write patterning technique on the nitrocellulose membrane of a lateral flow device. B – Schematic of a 4.5 mm wide LFD with 1 mm constriction in the middle, placed in a micro-well plate for testing with the PCT assay.

introduced between the deposition of the polymer and the illumination by the laser light, to allow for the polymer to soak through the thickness of the nitrocellulose membrane. We had previously optimized these parameters to ensure both the complete penetration of the polymer within the nitrocellulose membrane and subsequent full polymerization of the polymer structures. The fabrication conditions including the photopolymer deposition speed, the laser scanning speed and the time delay that we have used for the device processing herein are sufficient to fully polymerize the photopolymer producing impermeable polymeric structures. The photopolymer used was Desolite 3471-3-14 from DSM Desotech, Inc., Elgin, IL, USA, which is an acrylate-based photopolymer with a viscosity of 10,000 mPa s at 25 °C. The laser used for the LDW patterning process was a 405 nm continuous wave diode laser (MLDTM 405 nm, Cobolt AB, Stockholm, Sweden) with an output power of 60 mW. The dispensing platform used for the deposition of the photopolymer onto the nitrocellulose membrane was a PICO® PμlseTM system from Nordson EFD, UK.

2.3. Device assembly

The components (cellulose wicking pad and LDW-patterned nitrocellulose membrane reaction pad) of the lateral flow devices were prepared and then assembled onto a backing card for stability ensuring appropriate (2–3 mm) overlap between these components for uninterrupted fluid flow. The devices were then cut to size using a CM5000 guillotine cutter (Biodot).

2.4. Device testing

To evaluate the LFD, it was dipped in the well of a 96-well microtiter plate, as shown in Fig. 1B, that had a mixture of the sample (20 μL), (commercially available human serum spiked with procalcitonin antigen), the detection antibody and the streptavidin-modified 40 nm AuNPs. The LFD was then left to stand for 3 min until the entire mixture in the well had wicked through the length of the device, to the top of the wicking pad. The device was then dipped into another well that contained 20 μL of PBS solution for a further 5 min to allow for any unbound reagents to be wicked through to the end of the device, thereby minimizing or eliminating any background color that might develop across the device.

3. Results

Here we report the results from several parameters investigated in the optimization of a constriction for enhanced sensitivity lateral flow devices. The following parameters were investigated and are shown below:

A. Parameter 1: Position of the constriction within the flow path, shown in Fig. 2A. Firstly, the distance of the constriction from the sample inlet was changed and the time taken for the flow front to travel across the device was measured. These measurements were taken at 5 mm intervals along the length of the device until the flow front reached the end of the test – defined as the end of the nitrocellulose membrane where it meets the wicking pad. Then the test line color intensity was measured for each constriction position and the results compared.

B. Parameter 2: Position of the test line within the flow path, shown in Fig. 2B. The position of the test line within the flow path was investigated, independent of the constriction position. Several test line positions were investigated, and the test line color intensity was recorded for each position.

C. Parameter 3: Position of the test line within the constriction, shown in Fig. 2C. The test line color intensity was recorded for each test line position measured within the constriction, at 1 mm intervals, including the angled openings at either end of the constriction.

D. Parameter 4: Double constriction. Finally, the use of a second constriction was investigated, shown in Fig. 2D. With the first constriction placed at the optimal position to control the flow rate, as determined from Parameter A. The second constriction to contain the test line as determined by parameters B and C. The time taken for the flow front to reach the end of the test and the test line color intensity were recorded for multiple concentrations of PCT and compared to devices with a single constriction and those without.

3.1. Parameter 1 - position of the constriction within the flow path

As previously reported, the addition of a constriction to an LFD can enhance the sensitivity of the assay [9]. Therefore, in the first instance we explored different positions of the constriction relative to the inlet point to examine the effect this had on the a) speed of the flow front and time taken for the test to complete and b) the resultant color intensity of the test line.

The position of the constriction was systematically changed with respect to the sample inlet of the device and seven different constriction positions were trialed. Fig. 3A shows a schematic of the devices tested, labelled from ‘a’ to ‘g’ where the start of the constriction is at a distance of 13 mm–1 mm from the sample inlet respectively, decrementing by 2 mm for each subsequent device (‘b’ to ‘f’). Fig. 3B shows a photo of a device for the constriction position ‘e’ for reference.

The hypothesis under investigation here is that the position of the constriction will affect the flow rate of the sample and reagents. This is important as it means that there will be varying amounts of time available for the components of the immunoassay to bind for each

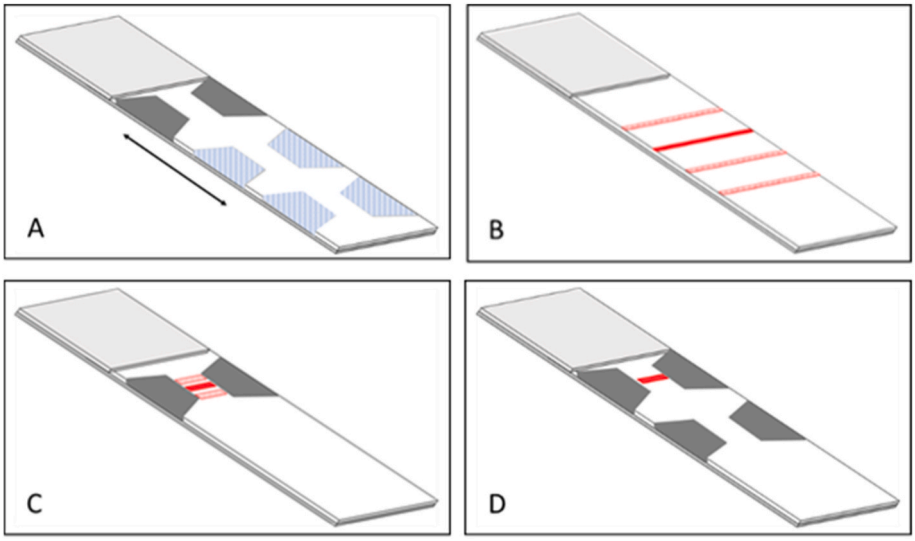

Fig. 2. A – Schematic showing position of the constriction within the flow path. B – Schematic showing position of the test line within the flow path. C – Schematic showing position of the test line within the constriction. D – Schematic showing the double constriction.

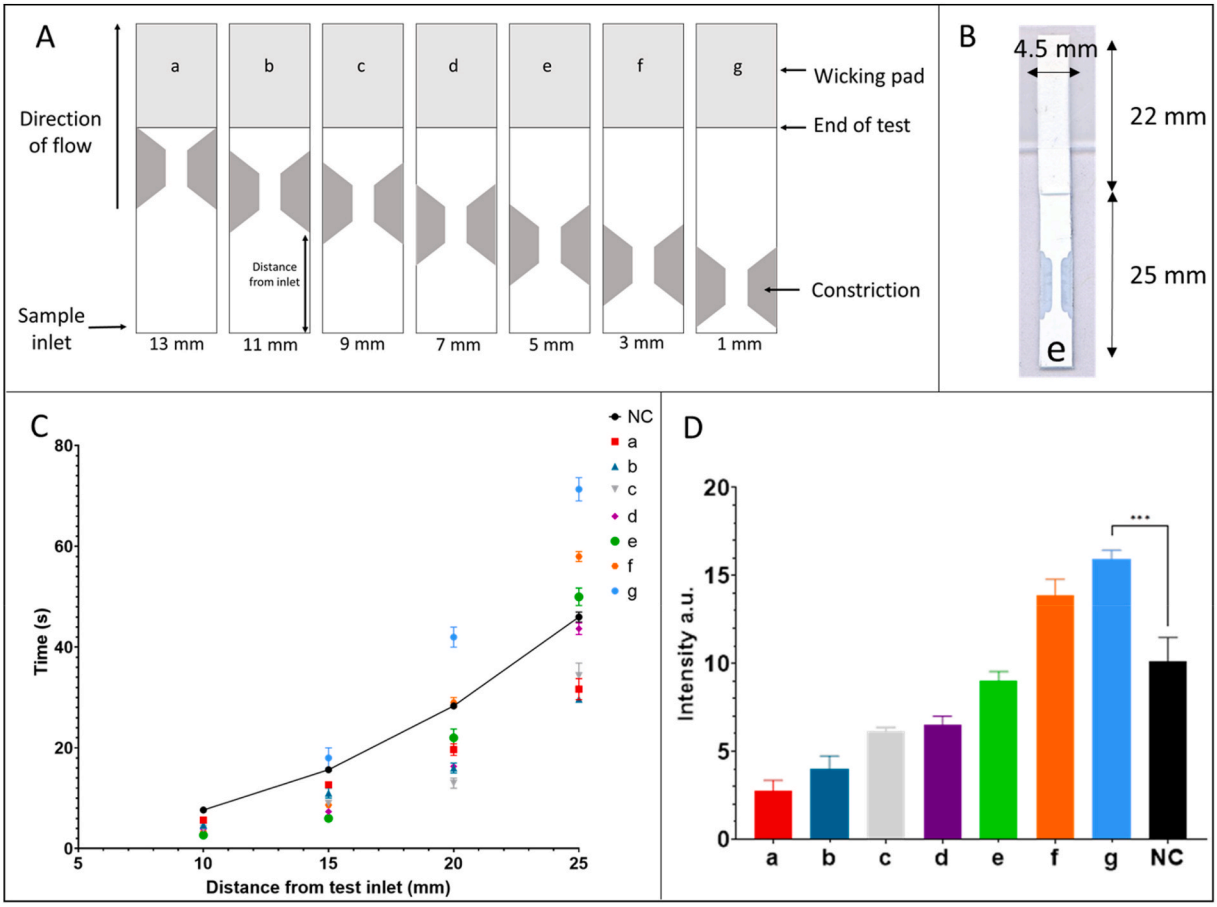

Fig. 3. A) schematic of seven different LFDs labelled a-g each with a constriction at a different position with a being the furthest from the sample inlet and g the closest. B) A photo of a LFD with constriction in position e. C) The results for the time taken for the flow front to travel along the length of the LFD. Here the time taken for the flow front to travel along the LFD was measured at several intervals from the sample inlet till the end of the test, for the seven constriction positions (a–g) and for a device with no constriction (NC) with a connecting line shown for NC as a guide to the eye. D) - Graph showing the mean test line color intensity with the mean plotted and error bars representing the standard deviation of three repeat measurements at 7 positions and a test with no constriction (NC). Differences were considered significant where $p < 0.05$ and calculated from unpaired t-tests. The star rating represents and is proportional to the level of significance of the data. (For interpretation of the references to colour in this figure legend, the reader is referred to the web version of this article).

different constriction position. The binding kinetics of the antibodies are crucial for the LOD of the assay and therefore this is a parameter that must be optimized to enhance the test sensitivity.

It was observed that over the length of the LFD the disparity in time between the different constriction positions became more significant as the flow front moved closer towards the end of the device, where the nitrocellulose membrane meets the wicking pad (at a distance of 25 mm). The constriction in position 'g', which was closest to the sample inlet, shows the greatest increase in time taken for the test to complete compared to the other positions and also when compared to a test with no constriction (NC). As seen in Fig. 3C, the black line represents the reference time of a device with no constriction, with the time for some constriction positions falling above and some below this line. At a distance of 25 mm from the inlet, the positions closest to the sample inlet, 'e', 'f' and 'g' are above this line and therefore show that those positions of the constriction slow the overall time taken for the test to complete. The position closest to the sample inlet, 'g', shows the most deviation from the baseline with the slowest time.

It was clearly observed that the time taken for the flow front to reach the end of the LFD for the different constriction positions affected the resultant test line color intensity, and a slower rate of flow produced a higher test line intensity. This is the expected result as the components of the immunoassay have an increased incubation time with the sample prior to arrival at the test line, and the analyte-antibody complex will move slower over the test line giving more opportunity for binding and the formation of the analyte-antibody-capture complex that is essential for the production of the visible test line. Fig. 3D shows the test line color intensity values for each of the seven constriction positions and the LFD with NC.

Statistical analysis performed in GraphPad prism using the unpaired *t*-test shows that there is significant different between the test line color intensity for constriction position 'g' and not having a constriction (NC), shown in Fig. 3D by the three-star significance rating.

3.2. Parameter 2 - position of the test line within the flow path

The position of the test line within the flow path of the LFD is another parameter that can affect the LOD of the test. The position of the test line defines how long the conjugate antibody and the sample have to bind before they reach the test line, and the flow speed at the test line then dictates how much time the analyte-antibody complex has to bind at the pre-deposited capture antibody. In addition, the speed of the sample flow decreases over the length of the LFD; therefore, the flow rate will be slower towards the end of the test so the immunoassay components will have more time to bind. The hypothesis here therefore is that the further the test line is positioned from the sample inlet the higher the test line signal intensity will be. The results of this set of experiments to determine the optimal test line position, as determined by the highest test line color intensity, are shown in Fig. 4.

The results show that as the test line moved further up the test, the test line color intensity increases, and this is true up until 12 mm from the sample inlet. At 15 mm from the sample inlet, however, the test line color intensity is lower, similar to having the test line placed at 3 mm from the sample inlet. This could be a result of the effect that the wicking pad has on the overall flow rate. Once the flow front reaches the wicking pad the flow will increase as the wicking pad has greater absorbent capacity than the nitrocellulose membrane and also acts as a passive pump that accelerates the extraction of the oncoming fluid from the nitrocellulose membrane. In the case when the test line is at 15 mm and relatively close to the wicking pad, when the flow front reaches the wicking pad the rest of the sample which is yet to cross the test line, is wicked across the test line at a higher rate. Therefore, the analyte in the sample has less time to bind to the capture antibodies resulting in lower binding and a decrease in the test line color intensity. Therefore, the optimal position for the test line was chosen to be 12 mm from the sample inlet.

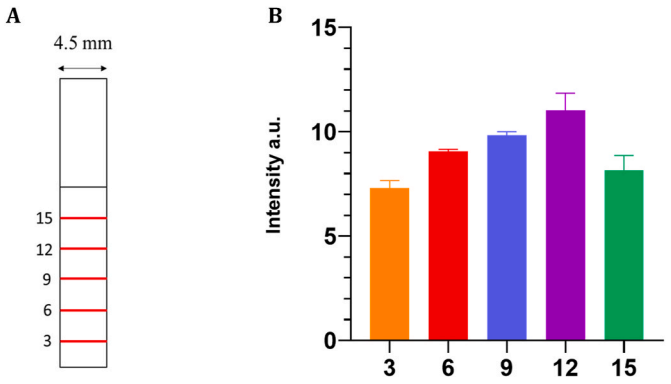

Fig. 4. A) Schematic of a non-constricted LFD showing the different positions of the test line that were investigated labelled by their mm distance from the sample inlet. The results are seen in B) where the test line color intensity for each different position is shown, with the mean plotted and error bars representing the standard deviation of three repeat measurements. (For interpretation of the references to colour in this figure legend, the reader is referred to the web version of this article).

3.3. Parameter 3 - position of the test line within the constriction

Previously it was determined [9] that the enhancement in test line color intensity is achieved not only by modulating the flow speed but also by reducing the test line width to allow for a greater volume of antibody-analyte complexes per unit area, and a 1 mm constriction gave the optimal results without overly compromising on test line visibility. Therefore, further to the investigation of test line position within the flow path we investigated the optimal position of the test line placement within the constriction. The constriction is 1 cm long including the angled inlet and outlet. We tested the position of the test line at 1 mm intervals through the length of the constriction to find the optimal position for increased test line color intensity.

The results for this are shown in Fig. 5 and it can be seen that the positions with the highest test line color intensity fall within the latter half of the constriction, from 5 mm to 9 mm inside the constricted path. When the flow front reaches the end of the constriction and spreads out

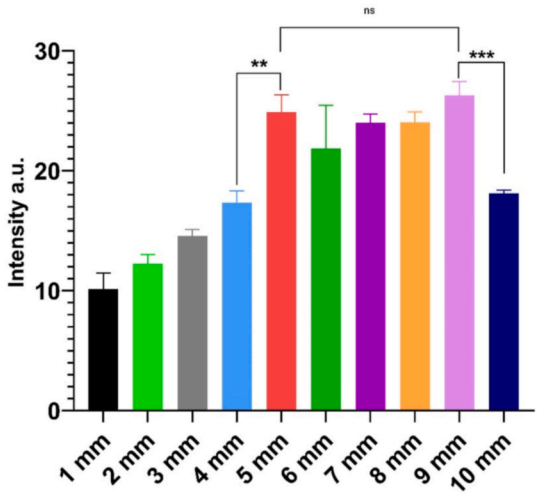

Fig. 5. Graph showing the test line color intensity for 10 different test line positions within the constriction characterized by the distance of the test line from the constriction inlet. Mean plotted with error bars representing standard deviation of three repeat measurements. Differences were considered significant where $p < 0.05$ and calculated from unpaired t-tests. The star rating represents and is proportional to the level of significance of the data or not significant (ns). (For interpretation of the references to colour in this figure legend, the reader is referred to the web version of this article).

from the 1 mm channel to the full 4.5 mm test the flow rate is slowed as the sample fills the larger area of nitrocellulose membrane. As the flow front dictates the rate of the subsequent sample flow, once the flow front reaches the end of the constriction the remaining sample will move more slowly through the constriction. It is important that the flow rate, when moving over the test line, is optimal to ensure the maximum binding for the components of the immunoassay. When the flow initially enters the constriction is goes from a wider channel width to a narrower cross-section, leading to an increase in flow rate, which aligns with the results shown here as the test line color intensity was lowest for the positions closest to the start of the constriction. The peak of test line color intensity falls at a position of 9 mm from the constriction inlet. However, after statistical analysis, significance levels highlighted in Fig. 5 with an asterisk rating of significance, was performed it was found that there was no significant difference in test line color intensity for the values collected from 5 mm to 9 mm but the difference in test line color intensity from 4 mm to 5 mm was significant and so was the change from 9 mm to 10 mm. Therefore, the optimal position was chosen as 9 mm.

3.4. Parameter 4 - double constriction

Having performed the experiments to optimize the parameters for a single constriction, the next logical step was to increase the number of constrictions, and so this last set of experiments was performed with two consecutive constrictions. The initial results from the position of the constriction within the flow path indicated that the best position for the constriction, to have the largest influence on controlling and slowing the flow rate, was at the position closest to the sample inlet. However, the test line position experiments dictated that the test line would not be ideally positioned near the test inlet but much closer to the end of the device. Our previous experimentation gave us the knowledge that the test line color intensity was maximized when the test line was placed within the 1 mm constriction and therefore combining this information with our acquired results a double constriction geometry was developed.

Fig. 6A shows one such example of a double constriction geometry. The initial constriction serves to slow the flow rate for the entire test to allow the components of the immunoassay more time to react. The hypothesis here is that the expected enhancement in the intensity at the test line would be a consequence of two combined effects, namely a slower flow rate and increased incubation time of the reagents, and the larger sample volume per unit width of test line, to increase the chance of binding and the density of the gold nanoparticles respectively, both leading to increased test line color intensity.

We first measured the time for the flow front for all constriction

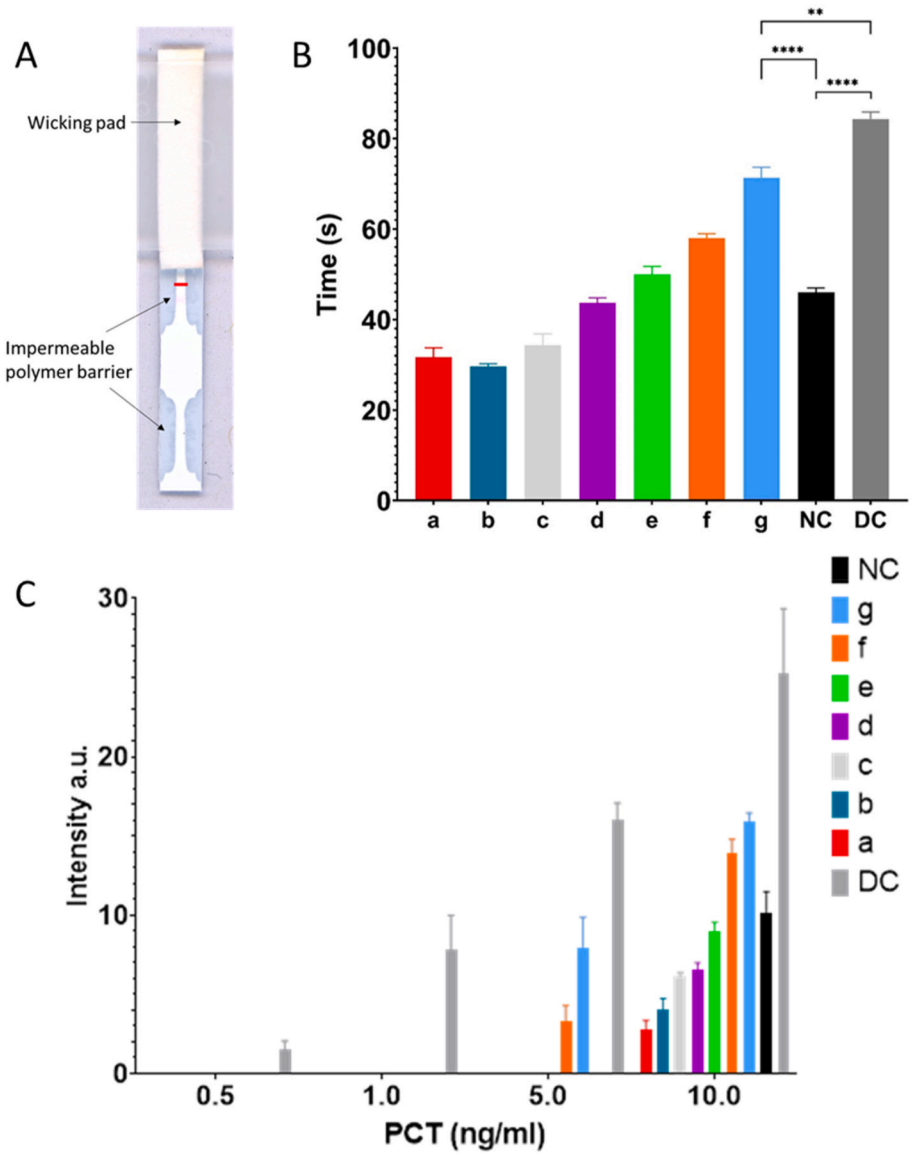

Fig. 6. A) – Scanned image of a single LFD with two (double) 1 mm width constrictions in the flow path (DC) with the test and control line. B) Graph showing the time (s) taken for the test to complete for the seven constriction positions, no constriction (NC) and double constriction (DC). Significance levels indicated. Differences were considered significant where $p < 0.05$ and calculated from unpaired t-tests. The star rating represents and is proportional to the level of significance of the data. Mean plotted with error bars representing the standard deviation of three repeat measurements. C) Graph showing the test line color intensity (s) for the seven constriction positions, no constriction (NC) and double constriction (DC). Mean plotted with error bars representing the standard deviation of three repeat measurements. (For interpretation of the references to colour in this figure legend, the reader is referred to the web version of this article).

positions as well as the LFDs with no constriction and double constriction, to travel from the sample inlet (t = 0) to the end of the nitrocellulose membrane. The results for this can be seen in Fig. 6B. It was observed that the positioning of a constriction close to the sample inlet decreases the flow rate and therefore increases the time for the test to complete. We had shown with previous experiments that 12 mm from the sample inlet was the optimal position for the test line and hence it was this that formed the basis of the next line of experimentation consisting of adding the second constriction to the flow path. The second constriction was added to enhance the effect of both slowing the flow and increasing the signal intensity due to the smaller capture site and concentrated accumulation of analyte-antibody complex. Statistical analysis of the data for devices that have the double constriction shows a significant increase in time taken for the test to complete, signified by the flow front reaching the end of the wicking pad ensuring that all the sample has passed over the entirety of the nitrocellulose membrane, when compared to that for devices with either a single constriction in position 'g' and or those with no constriction.

Finally, we measured the intensity of the test line for serum samples with a concentration of PCT of 10–0.5 ng/mL for all positions of the test line, the results for which can be seen in Fig. 6C.

The test line color intensity for the double constriction shows significant improvement, with an increase of 159% (mean value) compared to the device with no constriction. This equates to an improvement in the LOD from 10 ng/mL to 1 ng/mL when compared to that for devices with no constriction and from 10 ng/mL to 5 ng/mL for devices 'g' with a constriction positioned at 1 mm from the sample inlet, with a small visible signal at 0.5 ng/mL as shown in Fig. 6C. The signal at 0.5 ng/mL is faint and although it can be picked up with the scanner it cannot be viewed with the naked-eye and therefore the LOD for the double constriction is 0.5 ng/mL but the limit of quantification (LOQ) for naked eye reading is 1 ng/mL. This is a 10-fold improvement from devices with no constriction and a 5-fold enhancement from devices with a single constriction.

4. Discussion

The principle of a lateral flow assay is that the analyte in the sample is transported along the test by capillary flow. As it passes through the nitrocellulose membrane and the reaction zone the molecules diffuse towards pre-deposited capture sites leading to the formation of the analyte-antibody complex. It is reported that the analyte diffusion through the porous membrane is much faster than the immunochemical reaction, hence why the analyte-antibody complex formation is the limiting step of the process which is key for producing the visible test line [34]. Therefore, controlling and optimizing the sample flow rate is a critical factor in optimizing the antibody binding kinetics and ultimately the sensitivity of the test.

From previous work carried out it had been identified that the addition of a constriction to the flow path of a standard LFD can enhance the sensitivity and improve the LOD. This occurs by a two-fold effect: the presence of a constriction in the flow path affects the overall flow rate of the sample within the test, increasing the time taken for the test to complete. Secondly, as the test line placed within the constriction has a smaller area compared to the standard device, it allows more sample to flow over this smaller test line area, meaning there is more sample volume *per unit width* of the test line. Therefore, the capture antibodies have a greater opportunity to bind to the analyte in the sample, leading to a higher intensity test line color intensity. This effect is particularly important at low concentrations for normal tests without any constrictions where binding occurs over the full ~ 5 mm wide test line would produce a signal that was much less intense.

To build on this finding it was first established that the position of the constriction should be further investigated. Therefore, seven different constriction positions were trialed. In the first instance each test was run, and the times taken for the flow front to reach several pre-defined positions along the test were recorded. This showed that the position of the constriction has an impact on the time taken for the test to complete. The constrictions in positions closest to the sample inlet showed the most significant slowing of the flow rate, with position 'g' showing an increase in time for the test to complete of 155% compared to not having a constriction in the flow path. This is a highly significant increase, as confirmed by statistical analysis. Next the test line color intensity was measured for 10 ng/mL of PCT for each constriction position. The results show that the increase in time taken for the test to complete does translate into an increase in test line color intensity, as position 'g' shows an increase of 157% in intensity compared to the device with no constriction.

The increase in time taken for the test to complete leads to an increase in test line color intensity due to increased time given for the sample to bind the conjugate antibody and for this complex to bind at the capture site. However, as it is known that some of the enhancement in sensitively occurs due to the test line being positioned within the constriction, this became an issue as the constriction placed so close to the sample inlet would not be a preferable position for the test line due to the time for the interactions between the conjugate antibody and the sample. The rate at which the flow front travels decreases across the length of the nitrocellulose membrane until the front reaches the wicking the pad which assists by further drawing the sample through the membrane at a faster rate. When we then investigated the optimal test line position the results showed a position of 12 mm from the sample inlet was preferable, much higher than the ideal position for the constriction, but not completely at the end of the device. This is because the wicking pad speeds up the flow rate once the front has reached that point meaning subsequent sample would be drawn over the test line much faster and have less time to bind to the capture antibodies. Therefore, to take advantage of both aspects of the constriction enhancement, a second constriction was introduced higher up the device to contain the test line whilst the first constriction in position 'g' acted to slow the overall flow rate of the test.

The addition of a second constriction shows a further decrease in flow rate and therefore increased time for the flow front to reach the end of the LFD. This decreased flow rate further shows improvement in the increased test line color intensity and consequently the LOD. This improvement is greatest when comparing an LFD with no constriction to the introduction of a single constriction, however the addition of a second constriction shows significant difference in both decrease of flow rate and increase of test line color intensity and subsequent LOD both compared to a single constriction and to an LFD with no constrictions.

We were able to see a clear improvement in the LOD from 5 ng/mL for a single constriction to 1 ng/mL for the double constriction. The observed enhancement of LOD is 5× that of a single constriction and although this may seem a small increase, in the context of the use for PCT in sepsis or pneumonia triage, the usefulness of devices with a LOD that is not 5 ng/mL but a lower value of 1 ng/mL is crucial for an effective diagnosis.

5. Conclusion

In conclusion, there is clear merit in altering the LFD architecture by adding more than a single constriction within the flow path to produce a sensitivity enhancement and a consequent improvement in the limit of detection. Our reported method employs technologies requiring minimal modification to the LFD structure and thus ensures that scale-up or mass manufacture would be possible with minimal added cost.

Credit author statement

Alice H. Iles: Writing, investigation. Peijun J. W. He: Editing, methodology. Ioannis N. Katis: Editing, methodology. Peter Horak: Editing, methodology. Robert W. Eason: Supervision, editing. Collin L. Sones: Supervision, editing.

Declaration of competing interest

The authors declare that they have no known competing financial interests or personal relationships that could have appeared to influence the work reported in this paper.

Acknowledgements

The authors acknowledge the funding received via the Engineering and Physical Sciences Research Council (EPSRC) Grant Nos. EP/N004388/1, EP/P025757/1, EP/M027260/1 and EP/S003398/1. The underpinning data for this paper can be found at https://doi.org/10.5258/SOTON/D2016.

References

[1] Y. Wu, Y. Zhou, Y. Leng, W. Lai, X. Huang, Y. Xiong, Emerging design strategies for constructing multiplex lateral flow test strip sensors, Biosens. Bioelectron. 157 (2020) 112168, https://doi.org/10.1016/j.bios.2020.112168.

[2] P.K. Drain, E.P. Hyle, F. Noubary, K.A. Freedberg, D. Wilson, W.R. Bishai, W. Rodriguez, I.V. Bassett, Diagnostic point-of-care tests in resource-limited settings, Lancet Infect. Dis. 14 (3) (2014) 239–249, https://doi.org/10.1016/s1473-3099(13)70250-0.

[3] K.M. Koczula, A. Gallotta, Lateral flow assays, Essays Biochem. 60 (1) (2016) 111–120, https://doi.org/10.1042/ebc20150012.

[4] H. Lim, A.T. Jafry, J. Lee, Fabrication, flow control, and applications of microfluidic paper-based analytical devices, Molecules 24 (16) (2019) 2869, https://doi.org/10.3390/molecules24162869.

[5] E. Eriksson, J. Lysell, H. Larsson, K.Y. Cheung, D. Filippini, W.C. Mak, Geometric flow control lateral flow immunoassay devices (GFC-LFIDs): a new dimension to enhance analytical performance, Research (Wash D C) 2019 (2019) 8079561, https://doi.org/10.34133/2019/8079561, 8079561.

[6] T.-T. Tsai, T.-H. Huang, C.-A. Chen, N.Y.-J. Ho, Y.-J. Chou, C.-F. Chen, Development a stacking pad design for enhancing the sensitivity of lateral flow immunoassay, Sci. Rep. 8 (1) (2018) 17319, https://doi.org/10.1038/s41598-018-35694-9.

[7] C. Parolo, M. Medina-Sánchez, A. de la Escosura-Muñiz, A. Merkoçi, Simple paper architecture modifications lead to enhanced sensitivity in nanoparticle based lateral flow immunoassays, Lab Chip 13 (3) (2013) 386–390, https://doi.org/10.1039/C2LC41144J.

[8] L. Rivas, M. Medina-Sánchez, A. de la Escosura-Muñiz, A. Merkoçi, Improving sensitivity of gold nanoparticle-based lateral flow assays by using wax-printed pillars as delay barriers of microfluidics, Lab Chip 14 (22) (2014) 4406–4414, https://doi.org/10.1039/c4lc00972j.

[9] I.N. Katis, P.J.W. He, R.W. Eason, C.L. Sones, Improved sensitivity and limit-of-detection of lateral flow devices using spatial constrictions of the flow-path, Biosens. Bioelectron. 113 (2018) 95–100, https://doi.org/10.1016/j.bios.2018.05.001.

[10] J. Le Bel, P. Hausfater, C. Chenevier-Gobeaux, F.-X. Blanc, M. Benjoar, C. Ficko, P. Ray, C. Choquet, X. Duval, Y.-E. Claessens, on behalf of the ESCAPED study group, Diagnostic accuracy of C-reactive protein and procalcitonin in suspected community-acquired pneumonia adults visiting emergency department and having a systematic thoracic CT scan, Crit. Care 19 (1) (2015) 366, https://doi.org/10.1186/s13054-015-1083-6.

[11] H. Lee, Procalcitonin as a biomarker of infectious diseases, Korean J. Intern. Med. 28 (3) (2013) 285–291, https://doi.org/10.3904/kjim.2013.28.3.285.

[12] P. Schuetz, M. Briel, M. Christ-Crain, D. Stolz, L. Bouadma, M. Wolff, C.-E. Luyt, J. Chastre, F. Tubach, K.B. Kristoffersen, L. Wei, O. Burkhardt, T. Welte, S. Schroeder, V. Nobre, M. Tamm, N. Bhatnagar, H.C. Bucher, B. Mueller, Procalcitonin to guide initiation and duration of antibiotic treatment in acute respiratory infections: an individual patient data meta-analysis, Clin. Infect. Dis.: Off. Publ. Infect. Dis. Soc. Am. 55 (5) (2012) 651–662, https://doi.org/10.1093/cid/cis464.

[13] L. Simon, F. Gauvin, D.K. Amre, P. Saint-Louis, J. Lacroix, Serum procalcitonin and C-reactive protein levels as markers of bacterial infection: a systematic review and meta-analysis, Clin. Infect. Dis. 39 (2) (2004) 206–217, https://doi.org/10.1086/421997.

[14] M. Meisner, Update on procalcitonin measurements, Ann Lab Med 34 (4) (2014) 263–273, https://doi.org/10.3343/alm.2014.34.4.263.

[15] S. Harbarth, K. Holeckova, C. Froidevaux, D. Pittet, B. Ricou, G.E. Grau, L. Vadas, J. Pugin, Diagnostic value of procalcitonin, interleukin-6, and interleukin-8 in critically ill patients admitted with suspected sepsis, Am. J. Respir. Crit. Care Med. 164 (3) (2001) 396–402, https://doi.org/10.1164/ajrccm.164.3.2009052.

[16] A. Holm, S.S. Pedersen, J. Nexoe, N. Obel, L.P. Nielsen, O. Koldkjaer, C. Pedersen, Procalcitonin versus C-reactive protein for predicting pneumonia in adults with lower respiratory tract infection in primary care, Br. J. Gen. Pract. 57 (540) (2007) 555–560.

[17] F. Keramat, H.R. Ghasemi Basir, E. Abdoli, A. Shafiei Aghdam, J. Poorolajal, Association of serum procalcitonin and C-reactive protein levels with CURB-65 criteria among patients with community-acquired pneumonia, Int. J. Gen. Med. 11 (2018) 217–223, https://doi.org/10.2147/ijgm.S165190.

[18] J. Hedlund, L.O. Hansson, Procalcitonin and C-reactive protein levels in community-acquired pneumonia: correlation with etiology and prognosis, Infection 28 (2) (2000) 68–73, https://doi.org/10.1007/s150100050049.

[19] P.P. Galanis, P.J.W. He, I.N. Katis, A.H. Iles, A.J.U. Kumar, R.W. Eason, C.L. Sones, Local photo-polymer deposition-assisted fabrication of multilayer paper-based devices, Sensor. Actuator. B Chem. 322 (2020) 128574, https://doi.org/10.1016/j.snb.2020.128574.

[20] P.J. He, I.N. Katis, R.W. Eason, C.L. Sones, Laser-based patterning for fluidic devices in nitrocellulose, Biomicrofluidics 9 (2) (2015), 026503, https://doi.org/10.1063/1.4919629.

[21] P.J.W. He, I.N. Katis, R.W. Eason, C.L. Sones, Engineering fluidic delays in paper-based devices using laser direct-writing, Lab Chip 15 (20) (2015) 4054–4061, https://doi.org/10.1039/C5LC00590F.

[22] C.L. Sones, I.N. Katis, P.J. He, B. Mills, M.F. Namiq, P. Shardlow, M. Ibsen, R. W. Eason, Laser-induced photo-polymerisation for creation of paper-based fluidic devices, Lab Chip 14 (23) (2014) 4567–4574, https://doi.org/10.1039/c4lc00850b.

[23] P.J.W. He, I.N. Katis, R.W. Eason, C.L. Sones, Laser direct-write for fabrication of three-dimensional paper-based devices, Lab Chip 16 (17) (2016) 3296–3303, https://doi.org/10.1039/C6LC00789A.

[24] A.W. Martinez, S.T. Phillips, B.J. Wiley, M. Gupta, G.M. Whitesides, FLASH: a rapid method for prototyping paper-based microfluidic devices, Lab Chip 8 (12) (2008) 2146–2150, https://doi.org/10.1039/b811135a.

[25] E. Carrilho, A.W. Martinez, G.M. Whitesides, Understanding wax printing: a simple micropatterning process for paper-based microfluidics, Anal. Chem. 81 (16) (2009) 7091–7095, https://doi.org/10.1021/ac901071p.

[26] Y. Lu, J. Shi W Fau - Qin, B. Qin J Fau - Lin, B. Lin, Fabrication and characterization of paper-based microfluidics prepared in nitrocellulose membrane by wax printing, Anal. Chem. 82 (1) (2010) 329–335.

[27] P. Preechakasedkit, W. Siangproh, N. Khongchareonporn, N. Ngamrojanavanich, O. Chailapakul, Development of an automated wax-printed paper-based lateral flow device for alpha-fetoprotein enzyme-linked immunosorbent assay, Biosens. Bioelectron. 102 (2018) 27–32, https://doi.org/10.1016/j.bios.2017.10.051.

[28] K. Yamada, T.G. Henares, K. Suzuki, D. Citterio, Paper-based inkjet-printed microfluidic analytical devices, Angew. Chem. Int. Ed. 54 (18) (2015) 5294–5310, https://doi.org/10.1002/anie.201411508.

[29] L. Hecht, D. van Rossum, A. Dietzel, Femtosecond-laser-structured nitrocellulose membranes for multi-parameter Point-of-Care tests, Microelectron. Eng. 158 (2016) 52–58, https://doi.org/10.1016/j.mee.2016.03.020.

[30] F. Schenk, P. Weber, J. Vogler, L. Hecht, A. Dietzel, G. Gauglitz, Development of a paper-based lateral flow immunoassay for simultaneous detection of lipopolysaccharides of Salmonella serovars, Anal. Bioanal. Chem. 410 (3) (2018) 863–868, https://doi.org/10.1007/s00216-017-0643-9.

[31] J. Olkkonen, K. Lehtinen, T. Erho, Flexographically printed fluidic structures in paper, Anal. Chem. 82 (24) (2010) 10246–10250, https://doi.org/10.1021/ac1027066.

[32] G. Xiao, J. He, X. Chen, Y. Qiao, F. Wang, Q. Xia, L. Yu, Z. Lu, A wearable, cotton thread/paper-based microfluidic device coupled with smartphone for sweat glucose sensing, Cellulose 26 (7) (2019) 4553–4562, https://doi.org/10.1007/s10570-019-02396-y.

[33] P.-K. Kao, C.-C. Hsu, One-step rapid fabrication of paper-based microfluidic devices using fluorocarbon plasma polymerization, Microfluid. Nanofluidics 16 (5) (2014) 811–818, https://doi.org/10.1007/s10404-014-1347-5.

[34] N. Kockmann, Transport Phenomena in Micro Process Engineering, Springer, 2008, pp. 163–224.